Gamma-Ray Compton Scattering: Experimental Compton Profiles for He, N_2, Ar, and Kr

P. Eisenberger and W. A. Reed
Bell Laboratories, Murray Hill, New Jersey 07974
(Received 12 January 1972)

A technique is described for measuring Compton profiles using a Te^{123m} 160-keV γ-ray source together with a Li-drifted-germanium detector. By studying He and N_2, whose Compton profiles have been previously measured using x rays and theoretically calculated, it is found that the γ-ray technique gives results which agree with both the theory and the previous x-ray measurements. Measured Compton profiles for Ar and Kr are also presented. These results would have been almost impossible to obtain by the x-ray technique because of the large photoelectric absorption of the low-energy x rays. The Ar and Kr results are compared with atomic Hartree-Fock calculations and found to agree at $q=0$ within experimental error which is less than 1%. As a result of these studies, it is concluded that all elements and their compounds can now be studied by Compton scattering.

I. INTRODUCTION

There has been, in recent years, a resurgence in the use of x-ray Compton scattering to measure the momentum distribution of atomic,[1,2] molecular,[1-5] and solid-state[6-8] systems. Because of the large photoelectric absorption of the 10–20-keV x rays, these studies have been primarily limited to systems containing elements with atomic numbers less than 13, although some measurements have been reported on titanium.[9] These measurements have increased the interest in investigating the rest of the Periodic Table. Recently, measurements have been reported by Felsteiner *et al.*,[10] in which they used a 60-keV Am^{241} γ-ray source together with a Li-drifted-germanium [Ge(Li)] detector to measure Compton profiles. Unfortunately, their experiments provide no basis for evaluating the technique's accuracy and give no strong demonstration of the possible advantages of γ-ray Compton scattering.

We report results for Compton profiles of He, N_2, Ar, and Kr in which a 160-keV Te^{123m} γ-ray source was used together with a Ge(Li) detector. The results for He and N_2 are compared with previous x-ray experiments[1,2] and theoretical calculations.[3] The comparison reveals that if there is any difference between the x- and γ-ray results, it would be that the γ-ray results agree slightly better with the theory. However, both techniques agree within experimental accuracy for these low-atomic-number systems. New Compton-profile data for Ar and Kr is presented and compared with theoretical Compton profiles calculated from Clementi wave functions. Again, the agreement is good. The small deviations observed may be attributed to electron-correlation effects which are not included in the Clementi wave functions. The new data for Ar would have been very difficult to obtain by the x-ray method while the Kr data would have been almost impossible. It took only 3 days to measure Kr by the γ-ray technique while to get the same resolution and signal to noise with conventional x-ray sources it would have taken more than 1 yr. It is, in fact, a major conclusion of this work that by utilizing the γ-ray method, it is possible to measure the Compton profiles of all elements and their compounds.

In addition to presenting the above-mentioned data, a primary purpose of this work is to delineate the experimental approach used and discuss its advantages over both the x-ray and the 60-keV γ-ray techniques.

In Sec. II, the theory of Compton scattering will be briefly reviewed. Additional relativistic corrections are presented which become significant when using 160-keV photons instead of the 20-keV photons used in the x-ray studies. In Sec. III, the experimental method will be described including the data-reduction process itself. Also in that section the data for Compton profiles of He, N_2, Ar, and Kr will be given. In Sec. IV, the data will be compared with both theory and previous x-ray results, and the experimental approach used in this work will be compared with both the x rays and the 60-keV γ rays.

II. THEORY

The cross section for the inelastic or Compton scattering of electrons has been calculated for both free electrons[10,11] and bound electrons.[12] These results indicate that as long as the recoil energy of the electron E_R is large compared to the binding energy E_B, the impulse approximation is valid. If in addition, the incident energy is small compared to m_0c^2, the Compton cross section is given by

$$\frac{d\sigma}{d\omega\, d\Omega} = \left(\frac{d\sigma}{d\Omega}\right)_{\mathrm{Th}} \frac{\omega_1}{\omega_2}\left(\frac{1}{2\pi}\right)^3 \times \int n(\vec{p}_0) d^3p_0\, \delta\left(\omega - \frac{k^2}{2m_0} - \frac{\vec{k}\cdot\vec{p}_0}{m_0}\right) , \quad (1)$$

where

$$\left(\frac{d\sigma}{d\Omega}\right)_{\mathrm{Th}} = \left(\frac{e^2}{m_0c^2}\right)^2 (\vec{\epsilon}_1\cdot\vec{\epsilon}_2)^2 \left(\frac{\omega_2}{\omega_1}\right)^2$$

is the nonrelativistic Thompson cross section; ω_1 and ω_2 are the initial and final photon energies ($\hbar = 1$), respectively, with $\omega = \omega_1 - \omega_2$; $\vec{k}_1$ and $\vec{k}_2$ are the initial and photon moments, respectively; and $\vec{k} = \vec{k}_1 = \vec{k}_2$ is the momentum transfer. For isotropic or spherically averaged systems, Eq. (1) can be rewritten to take the form

$$\frac{d\sigma}{d\omega\, d\Omega} = \left(\frac{d\sigma}{d\Omega}\right)_{\mathrm{Th}} \frac{\omega_1}{\omega_2} \frac{m_0}{|k|} J(q) = C_x J(q) , \quad (2)$$

where

$$J(q) = 2\pi \int_q^\infty n(p_0)\, p_0\, dp_0 \quad (3)$$

is the Compton profile and

$$q = -\vec{k}\cdot\vec{p}_0/|k| \quad (4)$$

and

$$\int_{-\infty}^{\infty} J(q)\, dq = 1 \text{ per electron.} \quad (5)$$

Here $n(p_0)$ is the probability that an electron in the ground state of the system will have momentum p_0. In the impulse approximation, only ground-state properties of the scattering system are important. It is this feature which enables one to extract significant information about the momentum distribution of the electrons.

When the impulse approximation is valid, as in our work, but $(\omega_1/m_0c^2) \sim 1$, Eq. (1) must be recalculated in a completely relativistic formulation. Following Jauch and Rohrlich[13] the relativistic Compton cross section (in the approximation $p_0^2/m_0^2c^2$ terms are ignored and the case that the angle between k_1 and k_2, 2θ, equals 2π) is given by

$$\left(\frac{d\sigma}{d\omega\, d\Omega}\right)_{\mathrm{rel}} = \frac{r_0^2\, m_0c\omega_2(1+\omega_1/m_0c^2)\, B}{A_1(\omega_1+\omega_2)^2(1+\omega/m_0c^2)} J(q) , \quad (6)$$

where

$$B = \frac{\omega_1 A_1}{\omega_2 A_2} + \frac{\omega_2 A_2}{\omega_1 A_1} - \frac{4}{A_1 A_2} + \frac{4}{A_1^2 A_2^2} ,$$

$$A_1 = 1 + q/m_0c , \quad A_2 = 1 - q/m_0c .$$

The general relationship between the energy (eV) of the scattered photon and q (a.u.) is given by

$$q = -137\, \frac{\omega_1 - \omega_2 - \omega_1\omega_2(1-\cos 2\theta)/m_0c^2}{(\omega_1^2 + \omega_2^2 - 2\omega_1\omega_2\cos 2\theta)^{1/2}} . \quad (7)$$

It should be noted that we have defined q such that $q > 0$ lies on the high-energy side of the Compton profile.

The effect of the relativistic correction has been included in our results. The difference in magnitude between the relativistic and nonrelativistic cross sections is about 40% at the center of the profile while the difference in the variation between the two cross sections in the energy range of 88–123 keV ($-8 < q < 20$) is about 6%.

One proceeds experimentally by measuring the intensity of scattering at a fixed angle as a function of the energy of the scattered photons. The measured intensity $I(E_2)$ ($E_2 = \omega_2$) can be related to $J(q)$ by

$$I(E_2) = C_X S(E_2) J(q) , \quad (8)$$

where C_X is the correction for the energy dependence of the Compton cross section given in Eq. (6), $S(E_2)$ contains other energy-dependent terms whose origin is discussed in Sec. III, and E_2 is related to q through Eq. (7).

For high-Z elements where $p_0^2/m_0^2c^2$ is not negligible or when 2θ is not close to 2π, the single-valued relationships between energy and q and between intensity and $J(q)$ are destroyed. The cross section will explicitly contain terms that depend upon p_0 rather than q.

III. EXPERIMENT

A schematic of the experimental apparatus is shown in Fig. 1. The 1-Ci Te^{123m} source which emits 159.0-keV γ rays with a half-life of 120 days is contained in a stainless-steel cylinder with 0.010-in.-thick walls. The sealed source is inserted in a lead holder both to prevent γ rays from reaching the Ge(Li) detector directly and to

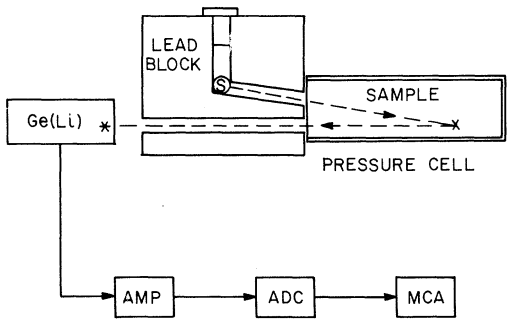

FIG. 1. Schematic diagram of experimental apparatus. The lead block is 5×5×5 in., S is the Te^{123m} source, Ge(Li) is the detector, AMP is the amplifier, ADC is the analog-to-digital converter, and MCA is the multichannel analyzer.

fix the scattering geometry: 173° scattering angle, 10^{-3}-sr input-beam collimation, 5×10^{-4}-sr scattered-beam collimation. The He, N_2, Ar, and Kr were studied in the gaseous state while in a pressure cell which has been previously described.[2] For these studies, a $\frac{1}{8}$- in. -thick $\frac{3}{4}$-in. -diam beryllium window served as both the entrance window for the input beam and the exit window for the scattered beam. The window was placed so that only a small amount of scattering from it could reach the detector. He, N_2, and Ar were studied at a pressure of ~525 lbs/in.^{2} while Kr was studied at both 300 and 100 lbs/in.^{2} to check for the presence of systematic effects.

As briefly described in Sec. II, we are interested in knowing the energy distribution of the scattered radiation. The Ge(Li) detector together with a multichannel analyzer is our dispersion analyzing system. The Ortec $\frac{1}{2}$-cm-thick $\frac{1}{2}$-in. -diam planar Ge(Li) detector puts out a voltage pulse whose amplitude is proportional to the energy of the incident photon. A count is then stored in the multichannel analyzer, where the channel number is proportional to the size of the pulse and, therefore, the energy of the photon which hit the detector. The linearity, resolution, and efficiency of the detector system were experimentally determined in a manner described in the Appendix. The system was found to be linear to better than 0.5% over the entire energy range of interest. The gain of the detection system was arranged so that there was a 40-eV separation between channels of the multichannel analyzer. The resolution function R was found to be mainly Gaussian with a full width at half-maximum of 470 eV at 98 keV. In addition, a non-Gaussian component was found on the low-energy side which was attributed to detector inefficiency. The efficiency of the detection system $D(E_2)$ was considered to be energy dependent because of the partial transparency of the detector at the high energies used in this study.

Neglecting for the moment the question of resolution, the intensity of the scattered beam at energy E_2 stored as counts in channel N would be given by

$$I(E_2)=D(E_2)A(E_2)C\left.\frac{d\sigma}{dE}\right|_{E_2}+B(E_2)\ , \tag{9}$$

where $A(E_2)$ accounts for the effect of the absorption of the incident and scattered beams by a gas of thickness t and linear absorption coefficient μ, as given by

$$A(E_2)=\frac{1-\exp\{-t[\mu(E_2)+\mu(E_1)]\}}{\mu(E_2)+\mu(E_1)}\ . \tag{10}$$

C contains all the energy-independent factors such as source strength, collimation, and channel width, $(d\sigma/dE)|_{E_2}$ is the differential cross section

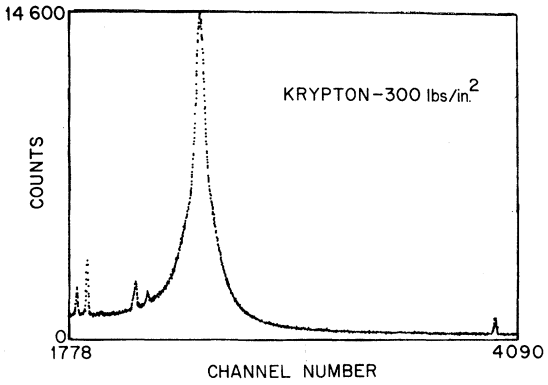

FIG. 2. Spectrum for Kr gas at 300 lbs/in.^{2} as recorded on multichannel analyzer after 2.9 days. Main peak is the Compton line; four small peaks at left are the Pb $K\alpha,K\beta$ lines; small peak on the right is the Rayleigh-scattered Te^{123m} line.

for the sample being studied which is described in Sec. II, and $B(E_2)$ is the sample-independent background intensity. The observed spectrum for Kr is shown in Fig. 2. Its main features are the Compton profile centered at 98 keV, lead fluorescence at 74 keV, and the flat background which extends way above the Compton-profile region.

The background $B(E_2)$ arises from two main sources: The first is due to photons from the source which never impinge upon the sample chamber but rather scatter from the lead holder itself. Included in this background is the cosmic-ray contribution. These background sources are easily measured by plugging up the exit port of the source. When this is done, a spectrum with the shape shown in Fig. 3 is found. Thus, in an actual experiment, one could measure the intensity of the background in the high-energy region and use the shape determined from Fig. 3 to subtract the background in the Compton-profile region. The second source of background arises from the sample chamber itself and includes Compton-scattering contributions from the beryllium window and a lead backstop which was placed at the end of the pressure cell. The beryllium-window component is also independent of the gas being studied and can thus be easily measured. By knowing the source strength and time of an experiment, its contribution can be easily removed from the measured spectrum. The lead contribution, on the other hand, does depend upon the sample being studied. Its strength and shape depends upon the absorption of both the input and the scattered beams by the gas. This background can be removed by using the observed lead fluorescence to scale the intensity of the lead contribution and using the known energy dependence of the absorption to modify the shape of the lead Compton background which is measured with no

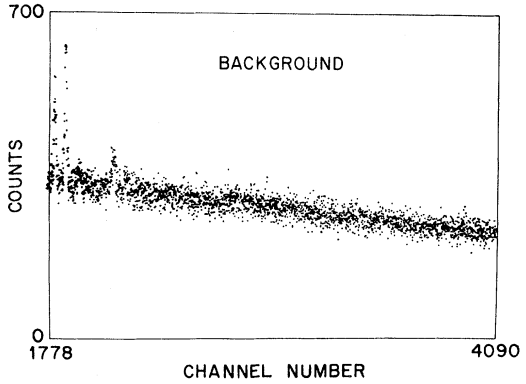

FIG. 3. Typical spectrum of background with source port closed after 3.2 days.

gas in the pressure cell.

For the very weak absorbing systems such as the He and N_2, all the background is easily removed by running first with the gas in the cell and then an equal time in the subtract mode with no gas in the cell. This procedure gave the same result, within experimental error, as that in which the measured background and calibration were used, as described above, to subtract the background electronically when processing the data. For Ar and Kr, the absorption was too strong to use the experimental subtraction. However, the agreement obtained by using the electronic subtraction in the weaker absorbing gases is a strong indication of one's ability to remove the background As a still further check in this, we measured Kr at two pressures (300 and 100 lbs/in.^{2}) in which the effects of absorption or any other sample-dependent effects are very different. The two experiments agreed within experimental error (see Table IV).

Still neglecting normalization and finite resolution considerations, one can obtain from the measured intensity $I(E_2)$ something related to the Compton profile $J(q)$. That is, using Eqs. (6), (9), and (10), one finds

$$J'_m(E_2) = \frac{I(E_2) - B(E_2)}{D(E_2)A(E_2)C_X(E_2)} \quad , \tag{11}$$

and Eq. (7) gives the relationship between E_2 and q.

The effects of finite resolution would be easily accounted for if one only had to consider the resolution of the detector. For as described in the Appendix, the effects of the detector are easily measured by letting a monochromatic γ-ray source impinge upon the detector. The measured line shape would then be the resolution function to be used in the deconvolution procedure. For our work, we used a standard Fourier-transform technique[14] for inverting the equation,

$$J'_m(E_2) = \int J'(E')R(E_2 - E')dE' \quad , \tag{12}$$

to obtain the resolution corrected $J'(E')$ from the measured profile $J'_m(E_2)$ knowing the resolution function $R(E_2 - E')$.

However, in these experiments, the finite collimation of the incident and scattered beam also contributes to the smearing of the Compton profile. An estimate of the magnitude of the smearing is obtained by differentiating the relationship between q and E_2 with respect to the scattering angle 2θ. Performing the differentiation at $q = 0$, the center of the profile, one finds from Eq. (7)

$$\frac{\partial E_2}{\partial 2\theta} = \frac{\omega_1^2 \sin 2\theta}{m_0c^2[1 + (\omega_1/m_0c^2)(1 - \cos 2\theta)]^2} \tag{13}$$

which for our collimation of $d\theta = \pm 4^\circ$ and our mean scattering angle $2\theta = 173^\circ$ gives a spread of ± 150 eV. The importance of having as large a 2θ as possible is indicated by Eq. (13). The distribution of angle is not exactly known. Assuming a Gaussian distribution, then one could, to first order, combine the effects of collimation and detector smearing by having the Gaussian part of the detector resolution function having a σ given by

$$\sigma = (\sigma_D^2 + \sigma_\theta^2)^{1/2} \quad , \tag{14}$$

where the detector contribution is σ_D and σ_θ is the collimation effect. Using $\sigma_D = 5.2$ (see the Appendix) and an estimate of σ_D, we calculated σ and used that value and Eq. (12) to analyze the He data. The He results were used as a test because it has the narrowest profile and consequently requires the largest resolution correction. It was found that using the trial $\sigma = 5.7$, a Compton profile for He was obtained which agreed with theory within the experimental error of 1% at $q = 0$. However, a systematic deviation was observed and thus the σ for the Gaussian part of the resolution function was trimmed slightly to a value of 6.0. This σ was then used in all the other data analyses.

The final results for He, N_2, Ar, and Kr are obtained following the resolution correction by taking the resulting $J'(E_2)$ and using the relationship between E_2 and q to normalize the spectrum according to Eq. (5) such that if

$$\int_0^\infty J'(q)\,dq = N \quad , \tag{15}$$

then

$$J(q) = \frac{\frac{1}{2}\text{ total number of electrons}}{N} J'(q) \quad .$$

The integration was performed on the high-energy side of the Compton profile because of the lack of fluorescent lines on that side and because of the smaller effects of resolution. The asymmetric

resolution function causes the low-energy side of the profile to be less reliable.

The integration depends sensitively upon the choice of $q=0$ which is theoretically determined by Eq. (7). However, because of the large size of the scattering volume, a very precise determination of the mean angle 2θ is difficult. To remove this difficulty, $q=0$ was determined by the condition that

$$\int_0^1 J(q)\,dq = \int_{-1}^0 J(q)\,dq \quad . \tag{16}$$

The $q=0$ point determined by Eq. (16) differed by less than 0.03 a.u. in q or 40 eV in energy from that found theoretically by Eq. (7).

The final results for the normalized and centered Compton profile for He, N_2, Ar, and Kr are given in Tables I–IV. These results are for the high-energy half of the Compton profile though both sides of the profile agreed fairly well throughout the region of $q=\pm 8$.

IV. DISCUSSION

A. Helium and Nitrogen

In Tables I and II we list the values of the Compton profiles for He and N_2 gases, which are predicted theoretically and measured by both x rays[1,2] and γ rays. The theoretical values were calculated from restricted-Hartree-Fock (RHF) atomic wave functions for He, and RHF wave functions for the N_2 molecule. In Table II we doubled the values taken from Ref. 3 and added the contribution of the 1s core electrons[15] since we normalized our data to 14 electrons/molecule.

TABLE I. Compton profile of helium.

q(a.u.)	Theory[a]	X-ray expt.	γ-ray expt.
0	1.070	1.066 ± 0.7%	1.071 ± 1.5%
0.1	1.057	1.052	1.058
0.2	1.017	1.012	1.019
0.3	0.955	0.954	0.958
0.4	0.878	0.876	0.881
0.5	0.791	0.789	0.795
0.6	0.700	0.700	0.705
0.7	0.611	0.612	0.616
0.8	0.527	0.527 ± 1%	0.533 ± 2.3%
0.9	0.450	0.448	0.456
1.0	0.382	0.382	0.388
1.2	0.271	0.275	0.274
1.4	0.190	0.195	0.188
1.6	0.134	0.137	0.129
1.8	0.095	0.098	0.092
2.0	0.068	0.067	0.069
2.5	0.031	0.027 ± 10%	0.030 ± 15%
3.0	0.015	0.008	0.013

[a] Theory taken from Ref. 1.

TABLE II. Compton profile of nitrogen (N_2).

q(a.u.)	Theory[a]	X-ray expt.	γ-ray expt.
0	5.343	5.327 ± 1%	5.271 ± 1.2%
0.1	5.299	5.277	5.228
0.2	5.169	5.142	5.100
0.3	4.964	4.924	4.896
0.4	4.689	4.631	4.627
0.5	4.364	4.286	4.309
0.6	4.006	3.914	3.959
0.7	3.629	3.523	3.593
0.8	3.251	3.153	3.227
0.9	2.887	2.803	2.874
1.0	2.546	2.476 ± 2%	2.545 ± 1.8%
1.2	2.958	1.934	1.982
1.4	1.503	1.527	1.550
1.6	1.168	1.230	1.230
1.8	0.922	0.997	0.989
2.0	0.751	0.821 ± 6%	0.805
2.5	0.504	0.542	0.524
3.0	0.378	0.390 ± 10%	0.400
3.5	0.295	0.301	0.299
4.0	0.234	0.244	0.238 ± 7%
5.0	0.148		0.147
6.0	0.083		0.086
7.0	0.053		0.048
8.0	0.034		0.030
9.0	0.022		0.019
10.0	0.015		0.009 ± 50%
15.0	0.002		0.000

[a] Theory calculated from twice the values in Ref. 2 with contribution of 1s core electrons added (see Ref. 15).

In both cases, the agreement is exceptionally good among the three sets of values. This is not too surprising for our He data since we slightly adjusted our resolution function to make $J(0)$ agree with theory. However, the agreement over the rest of the curve is also good. Our data for N_2, which were obtained with no adjustable parameters, agree with both the x-ray data and the theory. It should also be noted that we are able to obtain data out to $q=15$ whereas the x-ray data stop at $q=5$. This is due to the way the background is treated and will be discussed later. After considering the data on He and N_2, we feel that we have demonstrated that the γ-ray method can reproduce with at least equal accuracy Compton profiles of low atomic number which were previously measured by x rays.

B. Argon and Krypton

Tables III and IV and Fig. 4 contain our data for

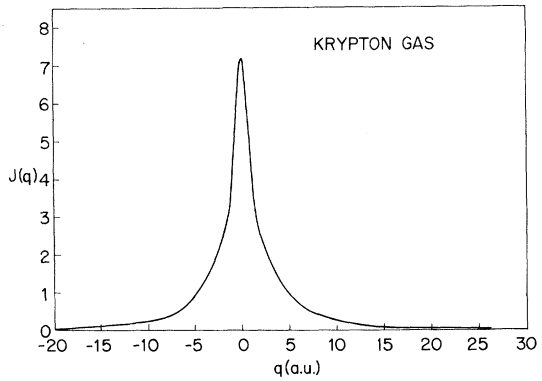

FIG. 4. Compton profile of Kr gas at 300 lbs/in.^{2}.

Ar and Kr as well as the theoretical values of the Compton profiles calculated using the atomic wave functions of Clementi.[16] For values of $q > 2$, the theory and experiment agree very well. Again, it should be noted that we are able to measure the profile at high values of q. For values of $q < 2$, the difference between the theory and experiment may be because of electron-electron correlation effects which are not included in the Clementi wave functions.

The data for Ar and Kr indicate that the γ-ray method can also produce reliable data for the higher-Z elements. In fact, Kr with a $Z = 36$ is the heaviest element to date whose Compton profile has been reported. Not only was it possible to measure Kr, but 1.5×10^4 counts were collected in the peak (0.8% statistical accuracy) in only 3 days.

TABLE III. Compton profile of argon.

q (a.u.)	Theory[a]	γ-ray expt.
0	5.052	5.058 ± 0.7%
0.1	5.028	5.022
0.2	4.950	4.917
0.3	4.812	4.749
0.4	4.608	4.526
0.5	4.369	4.259
0.6	4.028	3.960
0.7	3.690	3.643
0.8	3.328	3.319
0.9	2.982	3.000
1.0	2.658	2.697 ± 1.0%
1.2	2.108	2.164
1.4	1.701	1.753
1.6	1.417	1.461
1.8	1.221	1.264
2.0	1.084	1.129
2.5	0.873	0.904
3.0	0.736	0.744
3.5	0.621	0.634
4.0	0.520	0.534 ± 2.5%
5.0	0.351	0.366
6.0	0.249	0.260
7.0	0.177	0.181
8.0	0.130	0.137
9.0	0.098	0.104
10.0	0.075	0.078 ± 10%
15.0	0.025	0.025

[a]Theory calculated from Clementi wave functions (see Ref. 16).

TABLE IV. Compton profile of krypton.

q (a.u.)	Theory[a]	300 lbs/in.^{2}	γ-ray expt. 100 lbs/in.^{2}	av
0	7.228	7.222	7.188	7.205
0.1	7.194	7.168	7.135	7.152
0.2	7.085	7.016	6.988	7.022
0.3	6.888	6.777	6.757	6.767
0.4	6.595	6.465	6.453	6.459
0.5	6.216	6.1ט0	6.095	6.098
0.6	5.776	5.700	5.702	5.701
0.7	5.309	5.286	5.292	5.289
0.8	4.848	4.878	4.883	4.880
0.9	4.420	4.490	4.492	4.491
1.0	4.039	4.134 ± 1.2%	4.131 ± 1.7%	4.133
1.2	3.441	3.548	3.533	3.540
1.4	3.037	3.132	3.113	3.122
1.6	2.769	2.853	2.846	2.850
1.8	2.583	2.660	2.679	2.670
2.0	2.441	2.509	2.557	2.533
2.5	2.144	2.197	2.241	2.219
3.0	1.857	1.910	1.887	1.898
3.5	1.578	1.595	1.599	1.597
4.0	1.326	1.226	1.350	1.338
5.0	0.934	0.940 ± 2.5%	0.933 ± 3.5%	0.937
6.0	0.678	0.687	0.679	0.683
7.0	0.512	0.517	0.526	0.522
8.0	0.400	0.393	0.405	0.399
9.0	0.319	0.314	0.319	0.316
10.0	0.259	0.255	0.254	0.254
15.0	0.104	0.100	0.099	0.095
20.0	0.049	0.051 ± 25%	0.036 ± 30%	0.044
25.0	0.026	0.024	0.020	0.022
30.0	0.015	0.008	0.011	0.009

[a]Theory calculated from Clementi wave functions (see Ref. 16).

C. Comparison of γ-Ray and X-Ray Methods

Having demonstrated that the Compton profiles can be measured using high-energy γ rays, it is useful to compare the merits of γ rays *vis-à-vis* x rays. In Table V, we have listed the essential points of comparison. The first three columns are self-explanatory, and the fourth column is the factor by which the γ-ray method is faster than the x-ray method.

Source strength. Typically, an x-ray tube produces about 5×10^{14} photons/sec, whereas a 1-Ci nuclear source produces only 4×10^{10} photons/sec. Sources over 1 Ci are a bit difficult to handle. Thus, the x rays have an advantage of 10^4.

Solid angle. Although the solid angle for x rays can be varied depending primarily on the desired energy resolution, the solid angle used in Refs. 1 and 2 was ± 3° in one direction and ± 0.1° in the other. For the γ rays, the energy resolution is basically fixed by the detector so that the solid angle can be increased to ± 4° in both directions. Thus, the γ rays have an advantage of ~50.

TABLE V. Comparison of x rays and γ rays.

	x rays	γ rays	Time-decrease factor
Source strength	5×10^{14}	4×10^{10}	10^{-4}
Solid angle	$\pm3°$, $\pm0.1°$	$\pm4°$, $\pm4°$	50
Detecting efficiency	300 points, 1 at a time	all points, at once	300
Penetration depth (photoelectric, E^{-3})	1	10^3	10^3
Purity of beam	$K\alpha_1$, $K\alpha_2$ bremsstrahlung	δ function	
Background	guessed	measured	
Resolution Compton width at FWHM	$\frac{50}{250}$	$\frac{470}{2100}$	

Detecting efficiency. To determine a Compton profile using x rays, 300 points are typically measured, one point at a time. This is because the scattered beam is energy analyzed using a crystal which is set for only one energy at a time. The Ge(Li) detector, on the other hand, is a proportional detector and energy analyzes every photon received. Thus, the γ-ray method measures all points at once, which gives the γ rays a factor of 300 as the minimum gain in time. There is, however, another benefit from the Ge(Li) detector. Under our experimental conditions, we measured 700 points in nitrogen between $-8<q<15$ and 1670 points in Kr between $-8<q<40$. This higher density of points per profile in effect increased the statistical accuracy and resolution of the data. Thus, for N_2, 10^4 counts at $q=0$ would correspond to 2.3×10^4 counts if only 300 points had been measured.

Penetration depth. Over the range of energies 15–150 keV, the Compton cross section is essentially proportional to the atomic number Z whereas the photoelectric cross section is approximately proportional to Z^4/E^3. The ratio of Compton to photoelectric is then approximately E^3/Z^3. Since the γ rays have an energy of 160 keV compared to 17 keV for Mo x rays, the γ-ray method gains a factor of $\sim10^3$ in time for the same sample. The Z^{-3} term makes measurements on high-Z materials more difficult in all cases, but the higher energy of the γ rays makes some measurements feasible which are completely impractical at x-ray energies. Figure 5 illustrates quite well the tradeoff between energy and atomic number.

Purity of beam. Another major advantage of γ rays is that the incident beam may be considered a δ function in energy. This is in contrast to the x-ray beam which contains a $K\alpha_1$, $K\alpha_2$ doublet plus a bremsstrahlung background. Although techniques have been developed to remove these effects from the x-ray data, they still contribute to the uncertainty in the data.

Background. The background problem is much simpler with γ rays than with x rays. We have found that it is possible to either subtract the background experimentally or to measure our background independent of the sample and then subtract it, properly scaled, from our data. This procedure is impossible for the x rays since the major contribution to the background is due to the Compton scattering from the bremsstrahlung part of the input beam. The procedure usually followed is to subtract a uniform background, which gives a value for the Compton profile which agrees with some theory at high values of q. This, by its very nature, must lead to greater uncertainty in the data, especially at the higher values of q.

Resolution. Resolution is somewhat difficult to compare since it can be varied in the x-ray method, but is fixed by the quality of the detector for the γ rays. However, for comparison, we will take for the x rays 50 eV which was the resolution used in Refs. 1 and 2 and corresponds to using LiF (400) as an analyzing crystal. For He, the profile has

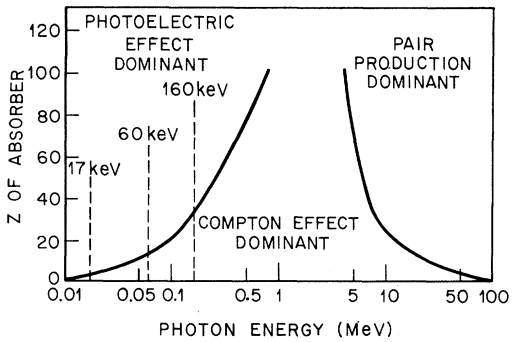

FIG. 5. Relative importance of photon absorption processes (see Ref. 17).

a full width at half-maximum (FWHM) of about 250 eV using 17-keV photons and FWHM of 2100 eV using 160-keV photons. Since our Ge(Li) detectors has a resulution of 470 eV in the Compton-profile region, both methods have comparable resolution.

C. Comparison with the 60-keV Source

Felsteiner *et al.*[10] and Batterman and McIntyre[19] have measured Compton profiles using 60-keV γ rays from an Am^{241} source. They have enjoyed a number of the advantages mentioned earlier which are associated with the Ge(Li) detector and a well-defined input energy. However, Am^{241} has several disadvantages compared to Te^{123m}. The most obvious disadvantage is that high-Z elements are harder to study using 60-keV radiation rather than 160-keV radiation. The second disadvantage is that, due to self-absorption, there is an absolute upper limit on the strength of the 60-keV line for a fixed source diameter. For example, 300 mCi is about the maximum strength that can be obtained in the 60-keV line from a source $\frac{1}{4}$ in. in diameter. A third disadvantage of Am^{241} is that impulse corrections can become important at 60 keV whereas they can be essentially ignored at 160 keV. Eisenberger and Platzman[12] have shown that corrections to the impulse approximation are $\sim\frac{8}{3}(E_B/E_R)^2$. Using an E_R for the Te and Am sources of 62 keV and 11.4 keV, respectively, and assuming an impulse correction of 25% or less, then E_B must be less than 25.9 keV for the Te and 4.9 keV for the Am. An $E_B \leq 25.9$ keV corresponds to a $Z \leq 47$ for $1s$ electrons and $Z \leq 98$ for $2s$ electrons. An $E_B \leq 4.9$ keV corresponds to a $Z \leq 22$ for $1s$ electrons, $Z \leq 52$ for $2s$ electrons, and $Z \leq 54$ for $2p$ electrons. However, at $Z=47$, the $1s$ electrons contribute only 4.2% of the area under $J(q)$ so that a 25% correction to the $1s$ part will cause at most a 1% error. At a Z of 22, the $1s$ contribution is 9% of the area of $J(q)$ and the error due to impulse corrections will be over 2%. The corrections for $2s$ electrons are at most 1% for elements with $Z \geq 98$ using the Te source but become 2% again for $Z \geq 52$ when using Am. Corrections for the $2p$ electrons become important for $Z \geq 54$ using Am but are never important for the Te source. A final disadvantage is that at 60 keV one has approximately one-half the resolution in q than at 160 keV.

V. CONCLUSIONS

In this paper, we have attempted to demonstrate that accurate Compton profiles can be measured using nuclear γ rays and a Ge(Li) detector, and that this technique has many significant advantages over the traditional x-ray methods. To demonstrate this new technique's ability to measure high-Z elements, we have presented data for Ar and Kr and compared it to values calculated from the atomic wave functions of Clementi. We have also argued in favor of using a Te^{123m} 160-keV source as an easy way to avoid corrections owing to the impulse approximation.

We feel that this new technique has unlimited possibilities since now the whole Periodic Table is available for study. Studies of alloys, phase changes, and chemical bonds are only a few of the areas in which Compton measurements can make significant contributions to our understanding. We also hope that this paper will stimulate more theoretical interest in calculating Compton profiles since now experimental data is readily available.

ACKNOWLEDGMENTS

We wish to thank Mrs. R. Fulton for extensive help with our computer programming and Dr. P. Platzman for many stimulating discussions. We also want to thank P. Polash for technical assistance.

APPENDIX: DETECTION SYSTEM

The Ge(Li) detector, amplifier, and multichannel analyzer will, for purposes of this section, be simply called the detection system.

Linearity

The detection system was found to be linear to better than 0.5% over the range of interest which included about 2500 channels or 100 keV. The linearity was tested by use of four sources: Fe^{55} (5.89 keV), Cd^{109} (88.0 keV), Co^{57} (122.0, 136.5 keV), and Te^{123m} (159.0 keV). During the course of the actual experiments, the linearity was preserved by use of a standard two-point stabilization scheme. The zero of the analog-to-digital converter was held fixed by locking on the Fe^{55} line while the gain was fixed by locking on the $K\alpha_1$ fluorescent line of lead. After each run, the two lines were inspected to verify that no drift had occurred during the experiment. The gain of the system was set to give a 40-eV separation between channels of the multichannel analyzer.

Efficiency

The efficiency of the detection system was defined for our study as the fraction of photons at a given energy which strike the detector that make a pulse which is stored in the multichannel analyzer. By this definition the efficiency $D(E_2)$ is just given by

$$D(E_2) = 1 - e^{-\mu(E_2)t} \quad , \tag{A1}$$

where $\mu(E_2)$ is the total linear absorption constant including Compton scattering for germanium at energy E_2 and t is the thickness of the detector

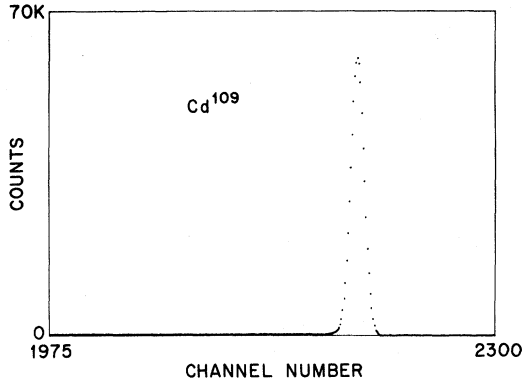

FIG. 6. Detector system's response to δ-function input at 88 keV.

which is 4.73 mm. The function $\mu(E_2)$ is given in the international x-ray tables.[19] Because of the high energies involved in our study, we decided to use the functional form for $\mu(E_2)$ given in those tables but fit the constants from experimental data. This was done by cutting a duplicate piece of germanium of the same dimensions as our detector and measuring its transparency at various energies. From this study, we obtained the following for $\mu(E_2)$:

$$\frac{\mu(E_2)}{\rho} = \frac{225.4}{\lambda_2^3} + \frac{76.8}{\lambda_2^4} + (2.47\times10^{23})\sigma_{KN}\,, \qquad \text{(A2)}$$

where $\lambda_2 = (12.398/E_2)$, σ_{KN} is the Klein-Nishina cross section,[19] and ρ is the density.

Resolution

We define the resolution of our detection system as its response to a δ-function energy spectrum. Since most gamma sources have an energy spread of less than 1 eV, they approximate very well a δ-function energy input into our system. The region of greatest interest as far as resolution is concerned is around 98 keV, the center of the Compton peak. The resolution in this region was measured by use of a Cd^{109} (88 keV) source. The spectrum seen in our analyzer is shown in Fig. 6. At first glance, it appears to be simply Gaussian; however, closer inspection shows that it has a pronounced asymmetry on the low-energy (low-channel) side, and that there is a small flat tail approximately 0.05% of the peak which extends for all practical purposes indefinitely to lower energy. The source of this tail is not completely understood but it is thought to arise from inefficiencies in the charge collection in the Ge(Li) detector. Using the measured Cd^{109} spectrum and the energy dependence of the Gaussian part of the resolution function to be proportional to $E_2^{1/2}$, the appropriate resolution function for photons of 98 keV is

$$R(E_2 - E') = \frac{1}{(2\pi\sigma_D^2)^{1/2}} \exp\left(\frac{(E_2 - E')^2}{2\sigma_D^2}\right) + R\,, \qquad \text{(A3)}$$

where

$$R = 0 \qquad \text{for } (E_2 - E') > 0$$

$$= \frac{0.004x}{1 + 0.9925x^2 + 0.004x^3} + 3.8\times10^{-5} \qquad \text{for } (E_2 - E') \le 0\,,$$

$$x = (E_2 - E')^2/36\,, \qquad \sigma_D = 5.2\,.$$

To be completely correct, one should use an energy-dependent resolution function (not only dependent on $E_2 - E'$); however, deconvolution with such a resolution function is very cumbersome. The small variation of only about 5% in the energy width of the Gaussian part of resolution function over the Compton profile ($q = \pm 4$ a.u.) and the small resolution effects present in our data (10% for He, 2% for Kr) make it unnecessary to use an energy-dependent resolution function.

[1]P. Eisenberger, Phys. Rev. A 2, 1678 (1970).
[2]P. Eisenberger, Phys. Rev. A 5, 628 (1972).
[3]P. Eisenberger, W. H. Henneker, and P. E. Cade, J. Chem. Phys. (to be published).
[4]P. Eisenberger and W. C. Marra, Phys. Rev. Letters 27, 1412 (1971).
[5]R. J. Weiss, J. Chem Phys. 52, 2237 (1970).
[6]W. C. Phillips and R. J. Weiss, Phys. Rev. 171, 790 (1968).
[7]R. J. Weiss and W. C. Phillips, Phys. Rev. 176, 900 (1968).
[8]M. Cooper and J. A. Leake, Phil. Mag. 15, 1201 (1967).
[9]R. J. Weiss, Phys. Rev. Letters 24, 883 (1970).
[10]J. Felsteiner, R. Fox, and S. Kahane, Phys. Letters 33A, 442 (1970); Solid State Commun. 9, 61 (1971); 9, 457 (1971).
[11]P. M. Platzman and N. Tzoar, Phys. Rev. 139, 410 (1965).
[12]P. Eisenberger and P. M. Platzman, Phys. Rev. A 2, 415 (1970).
[13]J. M. Jauch and F. Rohrlich, *Theory of Photons and Electrons* (Addison-Wesley, Cambridge, Mass., 1955), p. 228.
[14]T. Inonye, T. Harber, and N. C. Rasmussen, Nucl. Instr. Methods 67, 125 (1969).
[15]R. J. Weiss, W. C. Phillips, and A. Harvey, Phil. Mag. 17, 146 (1960).
[16]E. Clementi, IBM J. Res. Develop. Suppl. 9, 2 (1965).
[17]R. D. Evans, *The Atomic Nucleus* (McGraw-Hill, New York, 1955).
[18]B. W. Batterman and W. R. McIntire (private communication).

[19] *International Tables for X-Ray Crystallography*, edited by Caroline H. MacGillavry and Gerard D. Rieck, (The Kynoch Press, Birmingham, England, 1968), Vol. III, Sec. 3.2.

PHYSICAL REVIEW A VOLUME 5, NUMBER 5 MAY 1972

Low-Energy Theoretical Inelastic-Scattering Differential Cross Sections for the Process $He^+ + He \rightarrow He^+ + He(2\,^3S)$†

Ronald E. Olson
Stanford Research Institute, Menlo Park, California 94025
(Received 7 October 1971)

Coupled-channel calculations have been performed at 27.5, 30, and 50 eV for the reaction $He^+ + He \rightarrow He^+ + He(2\,^3S) + 19.81$ eV using presently available *ab initio* potentials for the two lowest $^2\Sigma_g^+$ states. The inelastic-scattering differential cross sections have been calculated at these energies and are compared with recent experimental results. Several features are distinguished on the calculated cross sections. All possess low-frequency Stückelberg oscillations and a higher-frequency oscillation due to the nuclear symmetry of the reactants. At the two lowest energies of 27.5 and 30 eV, inelastic rainbow-type oscillatory structure is also observed. The inelastic rainbow structure was due to the maximum on the excited-state potential and the closeness of the collision energy to the threshold for this reaction. The elastic differential cross sections were calculated at 50 eV, and perturbations due to the crossing of the inelastic channel were found superimposed upon the electron and nuclear exchange oscillations.

INTRODUCTION

The $He^+ + He$ elastic scattering has received considerable attention in recent years because of the availability of experimental data and the presence of *ab initio* potential calculations for the ground $^2\Sigma_u^+$ and $^2\Sigma_g^+$ states. Elastic-scattering low-energy experimental data showing both the electron-exchange and the nuclear-exchange oscillations were first presented by Lorents and Aberth.[1] This paper was followed by a detailed analysis of the cross sections by Marchi and Smith[2] using *ab initio* potentials.[3,4] Later, several authors deduced potentials from the scattering data[5,6] and improved *ab initio* calculations were performed.[7] The elastic scattering now seems reasonably well understood with its electron and nuclear exchange oscillations[8] and the perturbations due to the crossings of higher excited states.[9,10]

For the He_2^+ system, the importance of crossings leading to inelastic states was first pointed out by Lichten[11] and, since then, experimental measurements have shown quite large cross sections for many of these processes. Inelastic differential cross sections leading to the $He(2\,^3S)$ state have been observed from 37.5 to 300 eV by Lorents *et al.*[12,13] Baudon *et al.* have measured the cross sections at higher energies for excitation of the He* $(1s, nl)$ levels and also for some higher-lying states.[14]

Ab initio calculations for many of the excited potential levels have been calculated by Michels[15] and more recently by Bardsley.[16] Both calculations indicate that there is a crossing between the ground $^2\Sigma_g^+$ state and the first excited $^2\Sigma_g^{+*}$ state at $R \approx (1.4\text{–}1.5)a_0$ at a potential energy of approximately 0.81 a.u. or 22 eV. This crossing leads to $He(2\,^3S)$ excitation and is reasonably well isolated from the higher excited levels, so we can expect that, at energies close to threshold, this will be the dominant inelastic reaction and a two-state coupled-channel calculation will be justified.[17] Another interesting feature in the excited-state potential is that it possesses a maximum of about 0.88 a.u. or 24 eV at $R \approx 2.0a_0$, where a_0 is the Bohr radius. This is at an energy above the crossing-point energy so that the possibility exists for orbiting and rainbow-type phenomena. Also, the maximum is several eV above the endothermicity for this reaction, 19.81 eV, so that the threshold for scattering will be displaced above this value.

In the threshold energy range, 25–50 eV, the inelastic scattering will provide a very sensitive test of the *ab initio* potential calculations in the region about the crossing point. We have undertaken to calculate the cross sections and will compare them with recent experimental data that will be presented in more detail in a later paper.[18] Besides finding extreme sensitivity to the potentials used, several interesting features are observed on the calculated cross sections. Along with the usual Stückelberg oscillations arising from the interference between two different trajectories scattering to the same angle, there are the nuclear symmetry oscillations